The effect of a crystal field on density functional calculations of positron lifetimes in alkali halides

1997 J. Phys.: Condens. Matter 9 3583

(http://iopscience.iop.org/0953-8984/9/17/008)

J. Phys.: Condens. Matter **9** (1997) 3583–3600. Printed in the UK PII: S0953-8984(97)74071-2

The effect of a crystal field on density functional calculations of positron lifetimes in alkali halides

Keunjoo Kim† and Joseph G Harrison

Department of Physics, University of Alabama at Birmingham, Birmingham, AL 35294-1170, USA

Received 29 April 1996, in final form 25 September 1996

Abstract. A first-principles theoretical investigation of positron annihilation in alkali halide crystals is carried out using a simplified cluster-embedding scheme. The system is represented as a halide-centred cluster with basis functions only at the centre. The rest of the crystal is modelled in two ways: (i) point ions located at lattice positions; and (ii) frozen-orbital ions derived from an energy band calculation for the pure crystal. Calculations for both models are carried out within the self-interaction-corrected local spin-density approximation and by incorporating an electron–positron correlation functional. The effect of the model assumed on the calculated positron lifetimes is analysed by demonstrating the sensitivity of the results to the inclusion of the Madelung potential. A comparison of positron lifetimes of the ground state of the positron to lifetime components identified in experimental work on lithium and sodium halide systems is made.

1. Introduction

In the last few decades, density functional theory has rendered many-body calculations feasible. During this time, positron annihilation experiments have unquestionably established positron physics. The sensitivity of the positron to many-body structures has led to a wide range of applications to a variety of materials. Positron annihilation, in particular, has become an increasingly useful probe for the study of electronic states in a number of condensed-matter systems [1].

Recently, Puska and Nieminen have extensively reviewed the interesting topic of positron annihilation in solids and on solid surfaces [2]. The positron probe is outstanding for a wide range of applications within the areas of determination of the Fermi surface, and the search for vacancies in metals [3, 4]. In the fields of semiconductor physics and devices, the defect centres introduced during crystal growth can be identified using positrons, and slow-positron beams [5] can also be useful for determining the doping rate and the correct annealing temperature. Furthermore, the different annihilation rates can provide information about the identification of the impurity in the growing layer: carbon, oxygen, or boron. Generally, positron beams favour the formation of localized bound states at vacancies, substitutional and interstitial impurities, layered surfaces, and dislocations, so positron annihilation lifetimes for imperfect crystals are different from those for pure crystals [2, 6–9]. For these applications, it is of interest to explain how the crystal field

† Present address: Department of Physics and Semiconductor Physics Research Centre, Jeonbuk National University, Jeonju 560-756, Republic of Korea.

0953-8984/97/173583+18$19.50

influences the positron annihilation in pure-crystal structures such as those of alkali halides, in order to provide a reference for defect-associated positron annihilation.

A typical example of defect-associated positron annihilation is that involving F centres of coloured alkali halides [10]. The F centre consists of an electron which is localized on a halide-ion vacancy by the electrostatic forces of the remainder of the crystal. A positron in an F centre may undergo annihilation with one of the electrons of the neighbouring ions, but not with one of the electrons of the defect centre itself, as the electron spin is polarized parallel to that of the positron. This defect-related bulk annihilation of the positron is called pick-off annihilation [11]. In lifetime spectra, there is also evidence of a bulk-like trapped positron state in grown crystal layers, but the origin of this component and its exact lifetime are ambiguous [12–15]. In order to analyse the origin of the positron annihilation, a systematic investigation of the system of pure crystals is needed.

Positron lifetimes often hold key information about defect states of electronic structures. Although experimental spectroscopy may contain information about the electronic structure in solids, analysis of that information in terms of the specific structure of the electronic states may be difficult, because positron annihilation also occurs in defect-free and periodic-lattice states. Many of these problems of the data analysis could be resolved with theoretical calculations of the predicted positron lifetimes for the bulk state and defect-associated positron [16, 17]. In systems such as these, where the experimental characterization is incomplete or uncertain, parameter-free tools are essential.

A first-principles method for self-consistent calculations for the positron states in many-electronic systems has been developed [18]. There have been few attempts to calculate lifetimes from first principles for self-consistent charge densities, which include the electron–positron correlation [17]. In the atomic system, the positron correlation may provide a dramatic shift of the positron lifetimes, and reduce the discrepancy with respect to the experimental results for alkali halide crystals [19]. Furthermore, presumably the remaining discrepancy may originate from a crystal effect, which may change the forms of the overlapping densities of the electron and the positron.

In this paper, the aim is twofold: the systematic treatment of the crystal field by the Ewald method; and calculations of positron lifetimes for the ground state of the positron in the bulk state of the alkali halides LiF, LiCl, NaF, and NaCl, based on a first-principles calculation, to provide an initial reference for the defect analysis. The system is represented as a halide-centred cluster with basis functions only at the centre. The rest of the crystal is modelled in two ways: (1) point ions located at lattice positions; and (2) frozen-orbital ions derived from a linear-combination-of-atomic-orbitals (LCAO) energy band calculation for the pure crystal—the so-called LCAO embedded-cluster method [20–22]. Calculations for both models are carried out within the self-interaction-corrected local spin-density approximation (SIC-LSDA) of the three-component formalism of the density functional theory (DFT), incorporating a positron correlation functional. The dependence of the model of the crystal field on the calculated positron lifetimes is analysed. A comparison of the positron lifetimes for the ground state of the positron to lifetime components identified in the experimental work on lithium and sodium halide systems is made [19].

A brief review of the three-component formalism of the DFT is considered in section 2, and then, in section 3, the periodic crystal structure is outlined. A description of the computational procedure for the simplified embedded-cluster method for a centre-only cluster is provided in section 4. The phenomenology of the positron annihilation is briefly reviewed in section 5. The results for positron annihilation lifetimes are discussed and compared with experimental results, and finally brief conclusions are offered. Throughout this work, the Hartree atomic units (1 au = 27.2 eV and 1 au = 0.53 Å) have been used.

2. The density functional formalism

The density functional formalism for the electron–positron system is reviewed and extended to the periodic crystal structure. The total energy functional in three-component density functional formalism within the SIC-LSDA is written as

$$E_{\text{total}} = E_e + E_p + V_{ep} + E_e^{ep} \tag{1}$$

$$E_e = T_0 + V_{ext} + U_C + E_{xc} - U_e^{SIC} \tag{2}$$

$$E_p = T_0 - V_{ext} \tag{3}$$

and

$$U_e^{SIC} = \sum_i^{N_\sigma} (U_C[\rho_{i\sigma}] + E_{xc}[\rho_{i\sigma}]). \tag{4}$$

In the above expressions, the non-interacting component of the kinetic energy is denoted as T_0, the electron–nucleus interaction as V_{ext}, and the orbital densities of electrons as $\rho_{i\sigma}$ for the spin index $\sigma = \uparrow, \downarrow$. The electron exchange–correlation energy per electron for a uniform-density electron gas is denoted as E_{xc}, the electron–positron correlation energy in unit volume as E_c^{ep}, and the electron–electron and the electron–positron Coulomb interactions as U_C and V_{ep}, respectively.

Normalization constraints on the atomic orbitals are imposed via Lagrange multipliers $\epsilon_{i\sigma}$ in the usual way; the variational principle leads to the one-particle Kohn–Sham equations for the atomic orbitals of electrons and the single positron:

$$H_{i\sigma}^{\text{atom}} \Psi_{i\sigma}(\boldsymbol{r}) = \epsilon_{i\sigma}(\boldsymbol{r}) \Psi_{i\sigma}(\boldsymbol{r}) \qquad i = 1, \ldots, N_\sigma \tag{5}$$

$$H_{+}^{\text{atom}} \Psi_{+}(\boldsymbol{r}) = \epsilon_{+} \Psi_{+}(\boldsymbol{r}) \tag{6}$$

where

$$H_{i\sigma}^{\text{atom}} = -\frac{\nabla^2}{2} - \frac{Z}{r} + \int \mathrm{d}\boldsymbol{r}' \, \frac{\rho(\boldsymbol{r}')}{|\boldsymbol{r} - \boldsymbol{r}'|} - \int \mathrm{d}\boldsymbol{r}' \, \frac{\rho_+(\boldsymbol{r}')}{|\boldsymbol{r} - \boldsymbol{r}'|} + V_\sigma^{xc} + V_c^{ep-e} + \Delta V_{i\sigma}^{SIC} \tag{7}$$

$$H_{+}^{\text{atom}} = -\frac{\nabla^2}{2} + \frac{Z}{r} - \int \mathrm{d}\boldsymbol{r}' \frac{\rho(\boldsymbol{r}')}{|\boldsymbol{r} - \boldsymbol{r}'|} + V_c^{ep-p} \tag{8}$$

where V_σ^{xc} is the exchange–correlation potential of the electrons, and $\Delta V_{i\sigma}^{SIC}$ is the self-interaction correction term for the exact limit of an electron:

$$\Delta V_{i\sigma}^{SIC} = -\left(V_C[\rho_{i\sigma}] + \frac{\delta E_{xc}[\rho_{i\sigma}]}{\delta \rho_{i\sigma}} \right). \tag{9}$$

In the above expression, the orbital Coulomb potential is defined as $V_C[\rho_{i\sigma}]$, and we can use the exchange energy for the uniform electron gas:

$$E_{xc}[\rho_{i\sigma}] = \int \rho \epsilon_{xc}[\rho_{i\sigma}] \, \mathrm{d}\boldsymbol{r} \tag{10}$$

$$\epsilon_x[\rho_\sigma] = -\frac{3}{4}\left(\frac{6}{\pi}\right)^{1/3} \int \mathrm{d}\boldsymbol{r} \; [\rho_\uparrow^{4/3} + \rho_\downarrow^{4/3}]/\rho. \tag{11}$$

Furthermore, the correlation energy functional ϵ_c of the electrons is available from the work of Ceperley and Alder [23] as parametrized by Perdew and Zunger [24]. However, the SIC term from the orbital-by-orbital subtraction is independent of the electron–positron correlation term, because they are not identical. This means that the effective positron potential for the single-positron system is SIC free and consistent with the generalized Kohn–Sham equations introduced by Boronski and Nieminen [27]. The electron–positron

correlation energy functional per unit volume was analysed using the Sawada bosonic collective excitation by Arponen and Pajanne [25], and using the Fermi hypernetted-chain (FHNC) integral method with a Jastrow variational wavefunction by Lantto [26], as interpolated by Boronski and Nieminen [27]. At the limit of low electron densities, the effective positron potential approaches the positronium binding energy of -6.8 eV. These considerations are sufficient to deal with atomic electronic states, but the modification of the functional for the periodic system is needed. In the next section, the convergence of the crystal field, which is very sensitive to the positron lifetimes, is systematically achieved for the point-ionic and band-ionic potential limits.

3. The periodic crystal system

In a perfect crystal, the alkali halide lattice is constructed from two interpenetrating sublattices of the face-centred cubic (fcc) structure in which a halide ion is located at $\boldsymbol{R}_\nu$, and an alkali ion is placed at $\boldsymbol{R}_\nu + \boldsymbol{t}$. $\boldsymbol{R}_\nu$ is a translational vector of the fcc lattice, with the lattice constant a_0. $\boldsymbol{t}$ is the vector from a halide site to a nearest-neighbour alkali cation. The periodic crystal potential has been modelled as a modified point-ionic potential and an energy band-ionic potential as follows:

$$V_{\text{crys}}(\boldsymbol{r}) = \sum_{\nu=0} [V^H_{\text{ion}}(\boldsymbol{r} - \boldsymbol{R}_\nu) + V^A_{\text{ion}}(\boldsymbol{r} - \boldsymbol{R}_\nu - \boldsymbol{t})]. \tag{12}$$

For the modified point-ionic lattice, the potentials become

$$V^H_{\text{ion}}(\boldsymbol{r}) = \frac{1 - (Z^H + 1)\exp(-\alpha^H r^2)}{r} \tag{13}$$

$$V^A_{\text{ion}}(\boldsymbol{r}) = \frac{1 - (Z^A - 1)\exp(-\alpha^A r^2)}{r} \tag{14}$$

where Z^A and Z^H are atomic numbers of the alkali and the halide ions, respectively, and the exponential terms are negligible beyond the ionic radius R_{ion} (1.10 (Li^+), 1.81 (Na^+), 2.57 (F^-), and 3.42 (Cl^-)), and thus the relation $\exp(-\alpha R^2_{\text{ion}}) = \Delta = 10^{-6}$ gives the parameter α (11.42 (Li^+), 4.22 (Na^+), 2.09 (F^-), and 1.18 (Cl^-)). In a better approximation for the crystal potential, the fit of the crystal potential based on a band-structure calculation takes the form

$$V^H_{\text{ion}}(\boldsymbol{r}) = -\frac{Z^H}{r} e^{-\alpha^H_0 r^2} + \sum_i^{12} C^H_i e^{-\alpha^H_i r^2} \tag{15}$$

$$V^A_{\text{ion}}(\boldsymbol{r}) = -\frac{Z^A}{r} e^{-\alpha^A_0 r^2} + \sum_i^{12} C^A_i e^{-\alpha^A_i r^2} \tag{16}$$

where the Gaussian fitting parameters $C^H_i, \alpha^H_0, \alpha^H_i$, and $C^A_i, \alpha^A_0, \alpha^A_i$ are available from the energy band calculations [21].

The periodicity for the ionic crystal potential provides the potential form of the Fourier series:

$$V_{\text{crys}}(\boldsymbol{r}) = \sum_\nu V_{\text{crys}}(\boldsymbol{k}_\nu) e^{i\boldsymbol{k}_\nu \cdot \boldsymbol{r}} \tag{17}$$

so the Fourier coefficients of these potentials can be derived from

$$V_{\text{crys}}(\boldsymbol{k}_\nu) = \frac{1}{N\Omega} \int V_{\text{crys}}(\boldsymbol{r}) e^{-i\boldsymbol{k}_\nu \cdot \boldsymbol{r}} \, d^3\boldsymbol{r} \tag{18}$$

where Ω is the volume of a unit cell, N is the number of cells in the crystal, and $N\Omega$ is the volume of the entire crystal, and where

$$\boldsymbol{k}_\nu = m_1\boldsymbol{b}_1 + m_2\boldsymbol{b}_2 + m_3\boldsymbol{b}_3 \tag{19}$$

that is

$$\boldsymbol{k}_\nu = \frac{2\pi}{a_0}[l_x, l_y, l_z] \tag{20}$$

and

$$\boldsymbol{t} = \frac{a_0}{2}(1, 0, 0) \tag{21}$$

where l_x, l_y, and l_z are even or odd for the O_h^5 group of fcc crystals and $\boldsymbol{b}_1, \boldsymbol{b}_2$, and $\boldsymbol{b}_3$ are basis vectors of the reciprocal lattice for the fcc structure—that is, a bcc lattice. After changing the variables of the Fourier integrations and using $\boldsymbol{k}_\nu \cdot \boldsymbol{R}_\nu = 2m\pi$ and $\boldsymbol{k}_\nu \cdot \boldsymbol{t} = l_x\pi$, we obtain the following relations:

$$\frac{1}{N}\sum_\nu \mathrm{e}^{-\mathrm{i}\boldsymbol{k}_\nu\cdot\boldsymbol{R}_\nu} = 1 \tag{22}$$

$$\mathrm{e}^{-\mathrm{i}\boldsymbol{k}_\nu\cdot\boldsymbol{t}} = (-1)^{l_x}. \tag{23}$$

The Fourier coefficients can be obtained as

$$V_{\mathrm{crys}}(\boldsymbol{k}_\nu) = \frac{4\pi}{\Omega}[V_{\mathrm{ion}}^H - (-1)^{l_x} V_{\mathrm{ion}}^A] \tag{24}$$

with

$$V_{\mathrm{ion}}^H = \frac{1}{\boldsymbol{k}_\nu^2} - \frac{Z^H + 1}{\boldsymbol{k}_\nu\sqrt{\alpha^H}} D\left(\frac{|\boldsymbol{k}_\nu|}{2\sqrt{\alpha^H}}\right) \tag{25}$$

$$V_{\mathrm{ion}}^A = \frac{1}{\boldsymbol{k}_\nu^2} + \frac{Z^A - 1}{\boldsymbol{k}_\nu\sqrt{\alpha^A}} D\left(\frac{|\boldsymbol{k}_\nu|}{2\sqrt{\alpha^A}}\right) \tag{26}$$

where the Dawson function has been used:

$$D(x) = \int_0^\infty \mathrm{e}^{-t^2}\sin 2xt \ \mathrm{d}t.$$

The convergence of the matrix element

$$V_{ij}^{\mathrm{crys}} = \int \phi_i^*(\boldsymbol{r}) V_{\mathrm{crys}}(\boldsymbol{r})\phi_j(\boldsymbol{r}) \ \mathrm{d}^3\boldsymbol{r} \tag{27}$$

for the crystal potential can be examined. As an example, for a normalized s-type basis function, $\phi_i(\boldsymbol{r}) = N\exp(\alpha_i r^2)$, the matrix element of the crystal potential is written as

$$\langle\phi_i|V_{\mathrm{crys}}|\phi_j\rangle = \sum_\nu V_{\mathrm{crys}}(\boldsymbol{k}_\nu)\exp\left[-\frac{\boldsymbol{k}_\nu^2}{4(\alpha_i + \alpha_j)}\right]. \tag{28}$$

The convergence of the Fourier expansion is primarily determined by two factors: the Fourier coefficient $V_{\mathrm{crys}}(\boldsymbol{k}_\nu)$ and the exponential term. The Fourier coefficient of the crystal potential drops like $1/\boldsymbol{k}_\nu^2$, but the number of terms grows as $\boldsymbol{k}_\nu^2$ and will not converge unless the exponent helps. When $\alpha_i + \alpha_j$ is small ($\alpha_i + \alpha_j < 20$ with $\boldsymbol{k}_\nu \cong 31$), the matrix element will converge quickly, since the exponential term becomes smaller when $\boldsymbol{k}_\nu$ increases.

When $\alpha_i + \alpha_j$ is large ($\alpha_i + \alpha_j > 20$), the convergence of the Madelung potential is not rapid; since the exponential term is too large to neglect, the convergence depends on the Fourier coefficient $V_{\mathrm{crys}}(\boldsymbol{k}_\nu)$. So the convergence of the coefficient can be improved using Ewald's method [28] in which the short-range summation can be cut off by introducing

a short-range Gaussian screened potential $V_{\rm cut}$, which gives zero potential at the nearest neighbour. Now the crystal potential $V_{\rm crys}(\boldsymbol{r})$ can be written as a sum of two parts:

$$V_{\rm crys}(\boldsymbol{r}) = V_{\rm cut}(\boldsymbol{r}) + V_E(\boldsymbol{r}) \tag{29}$$

where the Ewald potential is defined by

$$V_E(\boldsymbol{r}) = V_{\rm crys}(\boldsymbol{r}) - V_{\rm cut}(\boldsymbol{r}) \tag{30}$$

and the cut-off potential is introduced as

$$V_{\rm cut}(\boldsymbol{r}) = \sum_{\nu=0}[V^H_{\rm cut}(\boldsymbol{r} - \boldsymbol{R}_\nu) + V^A_{\rm cut}(\boldsymbol{r} - \boldsymbol{R}_\nu - \boldsymbol{t})] \tag{31}$$

with

$$V^H_{\rm cut}(r) = \frac{-Z^H \exp(-\gamma r^2)}{r} \tag{32}$$

$$V^A_{\rm cut}(r) = \frac{-Z^A \exp(-\gamma r^2)}{r}. \tag{33}$$

The potential $V_{\rm cut}$ behaves like $-Z/r$ around each nucleus. It is a short-ranged function, dropping off to zero before r approaches the nearest-neighbour distance. The Ewald potential V_E is a relatively smooth function. It can be expanded in a Fourier series which converges with far fewer terms.

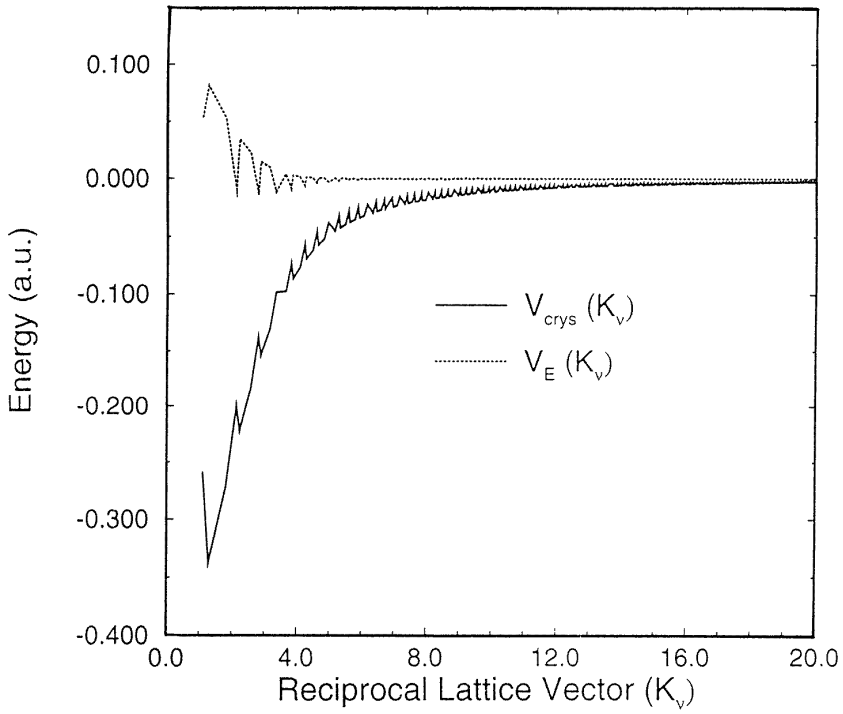

Figure 1. The convergence of the Fourier coefficients of the Ewald potential (1 au = 27.2 eV) in the modified point-ionic potential for LiCl with $\gamma = 1.0$. The crystal potential $V_{\rm crys}(\boldsymbol{k}_\nu)$ decreases as $1/\boldsymbol{k}_\nu^2$, while the Ewald potential $V_E(\boldsymbol{k}_\nu)$ decreases more rapidly, resulting in the rapid convergence of the lattice sum.

From the requirement that the Ewald and cut-off potentials have the same periodicity, the Fourier coefficients and the matrix element of the Ewald potential for the s-type basis function can be obtained:

$$V_{\rm cut}(\boldsymbol{k}_\nu) = \frac{4\pi}{k_\nu \Omega \sqrt{\gamma}} D\left(\frac{|\boldsymbol{k}_\nu|}{2\sqrt{\gamma}}\right)[Z^H - (-1)^{l_x} Z^A] \tag{34}$$

$$V_E(\boldsymbol{k}_\nu) = V_{\rm crys}(\boldsymbol{k}_\nu) - V_{\rm cut}(\boldsymbol{k}_\nu) \tag{35}$$

$$V_{ij}^E = \sum_\nu V_E(\boldsymbol{k}_\nu) {\rm e}^{-\boldsymbol{k}_\nu^2/4(\alpha_i+\alpha_j)}. \tag{36}$$

From the above equation, it is implied that while $V_{\rm crys}(\boldsymbol{k}_\nu)$ and $V_{\rm cut}(\boldsymbol{k}_\nu)$ decrease as $1/\boldsymbol{k}_\nu^2$, $V_E(\boldsymbol{k}_\nu)$ decreases more rapidly, as shown in figure 1. On substituting the Fourier coefficients $V_{\rm crys}(\boldsymbol{k}_\nu)$ and $V_{\rm cut}(\boldsymbol{k}_\nu)$ from equations (24) and (34), respectively, into equation (35), the lattice sum rapidly converges. The potential $V_{\rm cut}^H(\boldsymbol{r})$ with the parameter γ gives the $-Z^H/r$ behaviour at the halide site, and goes to zero for the near-neighbour distance. From the relation $R = \sqrt{2}t$, the following criterion is obtained:

$$\gamma \geqslant -\frac{4}{a_0^2} \ln\left(\frac{Z^A}{Z^H}\sqrt{2}\Delta\right) \tag{37}$$

where the tolerance factor is set to $\Delta = 10^{-6}$. Under this cut-off condition, energy minimization can be achieved rapidly, and the calculation of positron lifetimes shows non-sensitive and stable numerical results with the cut-off factor introduced. However, for values smaller than the cut-off factor, the total energy was not converged, and the calculated positron lifetimes were severely distorted and not consistent from one run to another.

The convergence problem of the matrix element for the energy band-ionic potential model can be addressed straightforwardly using the same procedure as was applied to the modified point-ionic potential model explained above. To simplify the calculation of the matrix elements via the analytical form of the matrix elements, the linear combination of Gaussian-type orbitals is useful; this can be optimized using the results of the atomic calculations made with the numerical atomic structure code [29]. With this orbital basis set, the self-consistent one-particle equations for the crystal system can be solved. The detailed computational procedure will be amplified in the next section.

4. The single-site embedded-cluster method

The three-component formalism of the SIC-LSDA adapted to the periodic crystal system is applied in order to investigate the positron annihilation process in alkali halides (LiF, NaF, LiCl, and NaCl) within the simplified cluster-embedding scheme. The system is considered as a halide-centred cluster with basis functions only at the centre. The rest of the crystal is simplified: it is modelled as point ions located at the lattice positions, or frozen-orbital ions derived from an LCAO energy band calculation for the pure crystal. The orbitals in the wavefunction are assumed to be expanded in terms of a convenient set of Gaussian-type orbitals (GTOs).

The total energy functional may be written as a sum of the atomic part including the atomic potential of the halide at the centre, and the Madelung potential energy of the periodic crystal lattice. From the functional derivative of the variational principle, the self-consistent formalism of the DFT leads to the one-particle Kohn–Sham equations:

$$H_{i\sigma}\Psi_{i\sigma}(\boldsymbol{r}) = \epsilon_{i\sigma}\Psi_{i\sigma}(\boldsymbol{r}) \qquad \sigma = 1, \ldots, N_\sigma \tag{38}$$

$$H_+\Psi_+(\boldsymbol{r}) = \epsilon_+\Psi_+(\boldsymbol{r}) \tag{39}$$

where

$$H_{i\sigma} = H_{i\sigma}^{\text{atom}} + V_{Ma} \tag{40}$$

$$H_{+} = H_{+}^{\text{atom}} - V_{Ma}. \tag{41}$$

Here, the Madelung potential is defined at the halide centre by $V_{Ma} = V_{\text{crys}} - V_{\text{centre}}$, and the total Hamiltonian includes the ionic crystal field in the atomic Hamiltonian. The matrix elements can be integrated by using GTO basis functions, and the matrix form of the Hamiltonian can be diagonalized to solve the Kohn–Sham equations.

For convenience, a simplified version of the LCAO embedded-cluster method [22] can be adopted for the analysis of the electron/positron structure of pure crystals. This code may also be useful for the analysis of the defect system of F-centre-related positron bound states. The essence of this method is that the eigensystem has the Hamiltonian of an infinite pure crystal and the basis set of a finite number of shells of ions around the halide position. This implies that while the expansion of the wavefunction in GTOs is limited to a finite number of shells, the Hamiltonian corresponds to the infinite system. Our simplified system is a halide-centred cluster with basis functions only at the first shell (central site), and is used to model positron bound states of the negative ion of the bulk site. The rest of the crystal potential in the Hamiltonian can be modelled and determined in the context of modified point ions located at the lattice positions, or the frozen-orbital ions derived from an LCAO energy band calculation for the pure crystal [20, 21].

In the context of the concept of the point defect centre in a crystal, the halide ion with a bound positron can be considered as a kind of defect centre in the pure crystal as the local limit of the positron state in perfect crystals. From this viewpoint, equations (38) and (39) can be solved with the LC-GTO embedded-cluster method by the construction of a point defect at the positron bound-halide-ion site. In other words, the Hamiltonian for the positron bound system may be analysed on the basis of a model in which the system is viewed as a pure-crystalline system with an embedded potential at the halide centre. The pure-crystal Hamiltonian H_{pc} includes the crystal kinetic energy and the crystal potential for the electron and the positron, respectively:

$$H_{pc}^{e} = -\frac{1}{2}\nabla^2 + V_{\text{crys}} \tag{42}$$

$$H_{pc}^{p} = -\frac{1}{2}\nabla^2 - V_{\text{crys}} \tag{43}$$

and the extra potential V_{emb} is composed of the effective potentials of the electron and the positron at the halide centre, written as

$$V_{emb}^{e} = -\frac{Z}{r} + \int \mathrm{d}\boldsymbol{r}' \, \frac{\rho(\boldsymbol{r}')}{|\boldsymbol{r} - \boldsymbol{r}'|} - \int \mathrm{d}\boldsymbol{r}' \, \frac{\rho_{+}(\boldsymbol{r}')}{|\boldsymbol{r} - \boldsymbol{r}'|} + V_{\sigma}^{xc} + V_{c}^{ep-e} + \Delta V_{i\sigma}^{SIC} - V_{\text{centre}} \tag{44}$$

$$V_{emb}^{p} = \frac{Z}{r} - \int \mathrm{d}\boldsymbol{r}' \, \frac{\rho(\boldsymbol{r}')}{|\boldsymbol{r} - \boldsymbol{r}'|} + V_{c}^{ep-p} + V_{\text{centre}}. \tag{45}$$

The density functional self-consistent iterative loop can be initiated from a zeroth-order approximation of the Hamiltonian of the crystal containing defects $\langle H_{dc} \rangle$, such as

$$\langle H_{dc}^{e(0)} \rangle = \langle H_{pc}^{e(0)} \rangle + \langle V_{emb}^{e(0)} \rangle \tag{46}$$

$$\langle H_{dc}^{p(0)} \rangle = \langle H_{pc}^{p(0)} \rangle + \langle V_{emb}^{p(0)} \rangle. \tag{47}$$

In the computational procedure, the perfect-crystal Hamiltonian matrix element $H_{pc}^{(0)}$, and $\langle V_{emb}^{(0)} \rangle$, are required to initiate iterations. The calculation for the infinite pure-crystal potential can be carried out by using the BANDAID package [30]. The Fourier coefficients

for the Coulomb and the Ewald potentials for the periodic infinite crystal have been installed into the perfect-crystal Hamiltonian matrix element.

Table 1. Gaussian basis exponents of the fluorine ion. These sets are optimized for crystal calculations for LiF and NaF from the numerical atomic structure results.

No of sets (i)	Electron	Positron
1	$0.150\,9536 \times 10^{5}$	$0.176\,6448 \times 10^{2}$
2	$0.216\,8112 \times 10^{4}$	$0.763\,7861 \times 10^{1}$
3	$0.356\,8040 \times 10^{3}$	$0.243\,3052 \times 10^{1}$
4	$0.100\,6477 \times 10^{3}$	$0.147\,0892 \times 10^{1}$
5	$0.304\,2323 \times 10^{2}$	0.738 9733
6	$0.972\,3098 \times 10^{1}$	0.185 0153
7	0.661 2085	$0.813\,0870 \times 10^{-1}$
8	0.605 6460	$0.395\,3731 \times 10^{-1}$
9	0.255 6460	$0.729\,7975 \times 10^{-2}$
10	0.100 8263	—
11	$0.705\,4373 \times 10^{-1}$	—
12	$0.118\,7524 \times 10^{-1}$	—
13	$0.500\,0000 \times 10^{-2}$	—

Table 2. Gaussian basis exponents for the chlorine ion for calculations of pure crystals of LiCl and NaCl.

No of sets (i)	Electron	Positron
1	$0.718\,4573 \times 10^{6}$	$0.171\,2508 \times 10^{3}$
2	$0.233\,3152 \times 10^{5}$	$0.511\,4676 \times 10^{2}$
3	$0.326\,8139 \times 10^{4}$	$0.392\,7008 \times 10^{2}$
4	$0.599\,8057 \times 10^{3}$	$0.136\,9680 \times 10^{2}$
5	$0.171\,2508 \times 10^{3}$	$0.454\,5725 \times 10^{1}$
6	$0.511\,4676 \times 10^{2}$	0.809 9507
7	$0.106\,8252 \times 10^{2}$	0.481 4303
8	$0.251\,9048 \times 10^{1}$	0.396 4695
9	0.595 2765	$0.966\,2527 \times 10^{-1}$
10	0.139 7643	$0.374\,8278 \times 10^{-1}$
11	$0.966\,2527 \times 10^{-1}$	$0.236\,9135 \times 10^{-1}$
12	$0.236\,9135 \times 10^{-1}$	$0.722\,0000 \times 10^{-2}$
13	$0.722\,0000 \times 10^{-2}$	$0.115\,8693 \times 10^{-2}$

Because of the conformal property of the GTOs, the basis functions fitted from numerical calculations for atoms perpetuate the advantage of simplifying the management of the multi-centred integration, which is encountered in matrix elements.

The single-GTO basis functions have been used with a finite number of exponents:

$$\Phi_i(r) = N_0 X \exp(-\alpha_i r^2) \tag{48}$$

where N_0 is a normalization constant, and α_i are the Gaussian exponents illustrated in tables 1 and 2. r is the distance from the centre of the function, and X represents angular factors used to specify the type (s, p, or d) of Gaussian function; X is 1 for zero-order Gaussians (s-type), and x, y, or z for first-order Gaussian functions (p-type). The size and composition of the basis set can be optimized by energy minimization as shown in figure 2 for the self-consistent density functional calculation. From these calculations, the self-consistent

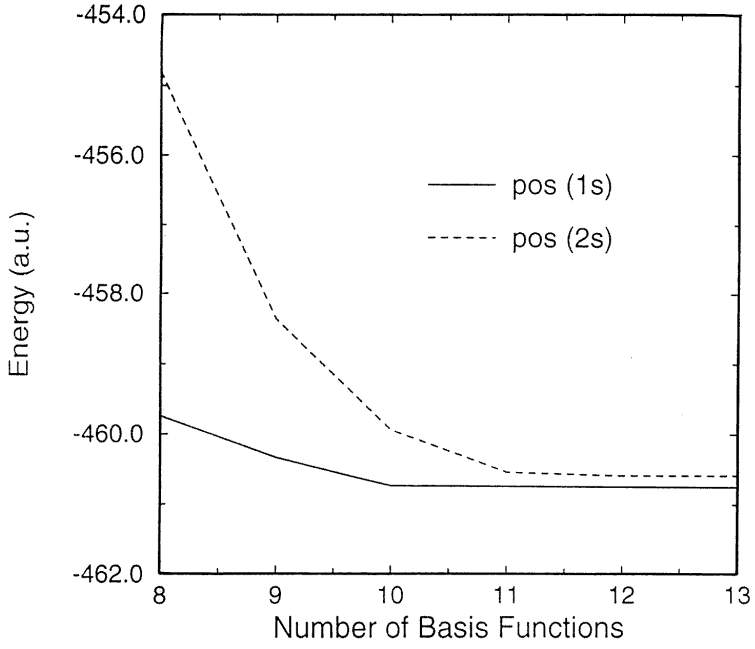

Figure 2. The energy minimization from optimized electron basis sets for positron states in the modified point-ionic potential of LiCl. Eleven basis functions of the positron are enough for total energy minimization.

eigenvectors directly lead to self-consistent densities, which are useful for positron lifetime calculations. General information about the positron annihilation is provided in the next section.

5. Positron annihilation

When a positron is incident on a solid, it may be thermalized on the bulk site or at a defect centre in crystals. The positron and the electron have the same mass, the same magnitude of electric charge, and the same magnetic moment. The charge quanta of the positron e^+ and the electron e^- are distinguished, with $e^+ = e^- = |e|$. In addition, the positron and the electron are distinguishable from each other, and thus do not comply with the exclusion principle. In thermal equilibrium with a medium of temperature T (K), the de Broglie wavelength of positrons, $2044.3/T^{1/2}$, is always large compared to the interatomic distances d in condensed matter, where $d \approx 5$ au, so $\lambda_+/d \gg 1$. Therefore, thermalized positrons in solids behave like waves as a requirement of the quantum behaviour of a particle.

The positron annihilates with an electron and emits quanta. Since the electron and the positron each have a spin of 1/2, there are two possibilities for the initial spin state. If particle spins are antiparallel, the total spin of the system is a singlet, $^1S_0$; if they are parallel, the system is a spin-triplet state, $^3S_1$.

Photons, on the other hand, each have a spin of 1, so the production of two photons would necessarily result in either a spin of 0 or a spin of 2. In order to obtain a state having a total spin of 1 and satisfying the linear momentum and energy conservation laws,

two photons must be emitted in antiparallel spin states in opposite directions, each with an energy of 0.511 MeV. However, three photons (3γ) will generally be emitted in the case of parallel spin states. The distribution of the angle among the three photons, and the annihilation energy of 1.02 MeV, are more complicated than in the two-photonic decay. The 3γ-decay is characterized by a typically small annihilation rate [31].

The observed radiation gives complete information about the state of matter, and the dynamics of the positron under the energy–momentum and spin conservation may be statistically analysed using the pair correlation function. The probability of pair annihilation increases with increasing probability of an electron being at a positron position. A key observable signal is the annihilation rate, which is proportional to the overlap of the electron and the positron densities that are self-consistently determined by using the procedure outlined in the previous section. For the two-photonic process, the annihilation rate can be written as

$$\lambda = \frac{1}{\tau} = \pi r_0^2 c \int \mathrm{d}\boldsymbol{r}\ \rho(\boldsymbol{r})\rho_+(\boldsymbol{r})g(0;\rho,\rho_+,\zeta) \tag{49}$$

where r_0 is the classical electron radius, ρ is the ground-state electron charge density, and ρ_+ is the positron charge density. If the electron and the positron are statistically independent, the annihilation rate just comes from the product of their densities. However, since they are not independent, especially in bound states, the rate is a sensitive measure of the electron–positron probability distribution. The pair correlation function $g(0;\rho,\rho_+,\zeta)$ gives a measure of the effect of quantum correlation between the electron and the positron at the original positron position in any polarization mode ζ. The positron annihilation rates were calculated for the two-photon channel at the absolute zero of temperature in the context of the unpolarized mode. The unpolarized pair correlation function has been taken from the interpolation scheme for the electron–positron correlation [27].

6. Results and discussion

The density functional calculations were carried out for bulk positron lifetimes in alkali halide crystals, such as LiF, NaF, LiCl, and NaCl. The potential is modelled in two ways: (i) point ions located at the lattice positions; and (ii) frozen-orbital ions derived from an LCAO energy band calculation for the pure crystal. The crystal system is modelled as a one-site embedded cluster for the infinite crystal, discussed in section 4. The equilibrium structures of the crystal lattices and lattice constants are used for the alkali halides. For this one-site approximation, the Hamiltonian defined represents the infinite crystal lattice, and the basis functions for the system are centred on the central anion site. The GTO basis set consists of the s and p single GTOs. This Gaussian set has been used in calculations of the pure-crystal Hamiltonian matrix element and the Madelung potential matrix element for both the electron and the positron. And also this set has been used for the self-consistent density functional calculation for the anion system; however, the electron and the positron have been represented using different basis sets for each crystal.

The energy, which is dependent on the choice of the Gaussian basis set, is minimized, and then the positron lifetimes are determined using the self-consistent densities of both of the electrons and the positron. The Madelung potential lowers the electron eigenstates via a relative contribution to the redistribution of electron states of the anion. For the positron, however, it is inferred that the shape of the potential on the neighbour lattices has a strong influence, because the positron is localized in the interstitial region due to the strong Coulomb repulsion between the nucleus and the positron.

6.1. The modified point-ionic potential

The point-ionic potential has been modified into a negative potential at each lattice point, because the thermalized positron in the crystal is strongly repelled by the nucleus at lattice points. The model potential becomes negative inside the ionic radius, and takes on the usual form of the point-ionic potential outside the radius.

Table 3. Gaussian calculations of positron lifetimes (ns) in negative atoms, with atomic structure information for the exchange-only potential (XO) calculation, the calculation including the electron–electron exchange–correlation potential and the electron–positron correlation potential (XC), and the calculation for the XC case with the pair correlation function g (EPC). The Hartree–Fock atomic calculation gives similar results to the XO case.

Atom	$nl(e^+)$	XO	XC	EPC	H–F[a]
F^-	1s	1.941	0.901	0.501	1.662
	2p	9.688	3.251	1.274	9.435
	2s	7.565	5.079	2.365	—
Cl^-	1s	4.247	1.260	0.581	4.018
	2p	12.63	2.819	1.066	12.46
	2s	713.92	7.592	3.581	—

[a]Farazdel and Cade [32].

The Gaussian calculations of the positron lifetimes in negative atomic systems are obtained, as illustrated on table 3, by adding the potential ingredients: the exchange-only potential (XO) calculation, the calculation including the electron–positron correlation potential and the electron–electron exchange–correlation potential without the electron–positron pair correlation function, i.e., $g = 1$ (XC), and the calculation for the XC case including the pair correlation function (EPC). It is worth noting that in the negative atomic system, positron lifetimes in the Gaussian calculation including the exchange-only potential (XO) without either the correlation potential or the crystal field are identical to the results of the XO numerical calculation made by the Hartree–Fock (H–F) method [32]. The Gaussian basis set is optimized using the potential generated by the numerical atomic code. The Gaussian basis set shows limitations as regards its ability to reproduce exactly the numerical results for the atomic system. In order to deal with multi-centre integrations of the crystal system, it is important to implement the Gaussian code with the optimized basis set for the XO calculation by using the potential of the numerical atomic structure calculation. The atomic results obtained with this Gaussian basis set provide a reference for assessing the crystal effect. The overall trends of the Gaussian atomic results agree qualitatively with those of the numerical atomic calculations.

The XO calculation including the Madelung potential shows a large shift of the positron lifetimes from the Gaussian atomic results. The XC calculation for the modified point-ionic potential model shows positron lifetimes shorter than those in the XO calculation; this shortening is produced by the shifting of the density as shown in figure 3. The strong inward attraction exerted on the positron density by the positron correlation potential in the vicinity of the nucleus is also present in crystal calculations. In the point-ionic crystal approximation, the positron density is spread out, and so slightly overlaps into the nearest Na^+ ions, by the distance of 4.4 au, in the NaF crystal. However, this density overlap with the adjacent atoms can be reduced in the energy band-ionic crystal calculation.

Another way to view the XC comparison of the atomic system and the crystal system is that the crystal effect becomes smaller than that in the XO calculation with the introduction

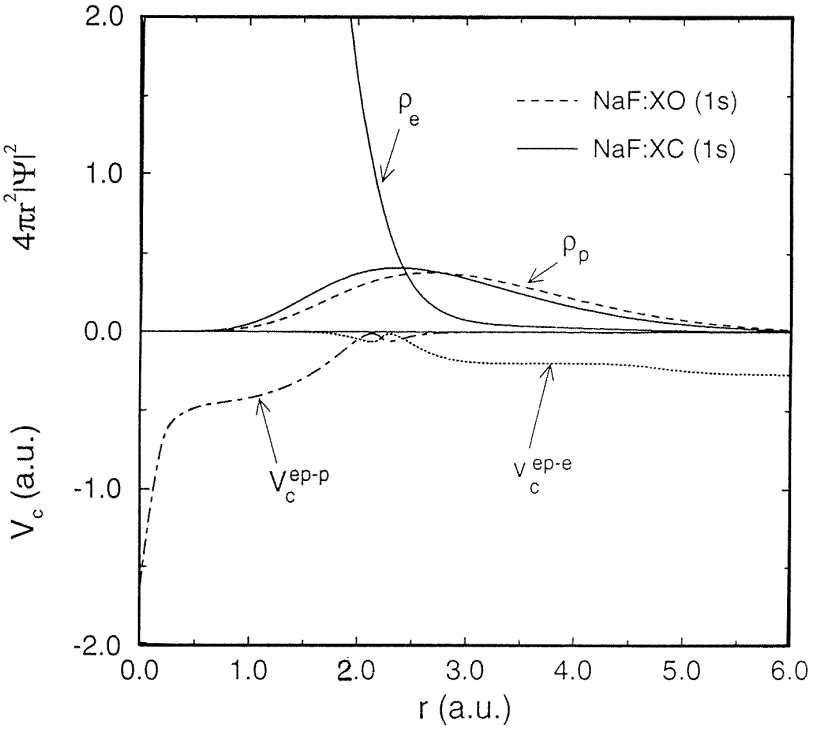

Figure 3. The positron correlation effect in the modified point-ionic potential model of NaF in terms of the atomic distance r (1 au = 0.53 Å). The positron correlation potential (1 au = 27.2 eV) (V_c^{ep-p}) in the vicinity of the nucleus attracts the positron density inward in the positron bound state in the crystal. The long-range limit of the electron correlation potential (V_c^{ep-e}) is the positronium binding energy of −6.8 eV.

of the electron–positron correlation effect. This implies that the Madelung potential is competing with the positron correlation potential. As shown in figure 4, with the inclusion of the electron–positron correlation potential in the XC calculation, the crystal field as a potential barrier to the positron strongly pushes the positron density inward, so the tail of the positron density of the ground state becomes localized within the range 7 au—smaller than the range in the atomic case: 10 au. The detailed information on the depth and width of the potential for a specific crystal gives the detailed difference of positron annihilation lifetimes.

For the 1s orbital of the positron in LiF, the contribution of the crystal effect to the lifetimes is slightly larger than that of the pair correlation effect, and it is of the same order in NaF. However, for both LiCl and NaCl, the pair correlation effect becomes larger. These features reflect that the shape of the crystal potential also influences the correlation effect. As the Madelung potential becomes shallower and wider, the correlation effect becomes more enhanced, without changing the shape of the correlation potential.

As the lattice constant becomes larger in alkali fluorides, the lifetime becomes larger for the ground state of the positron. This is also true for the alkali chlorides, as shown in table 4. The modified point-ionic calculations show the same order of magnitude of the positron lifetimes as the experimental data. However, there is still a large discrepancy between them, which may be attributed to the spread of the positron density due to the

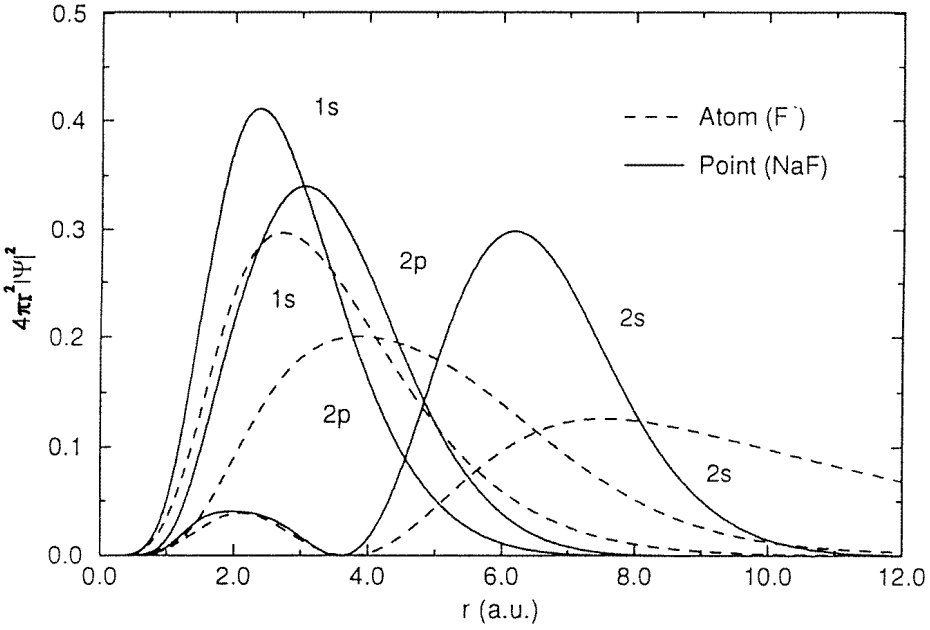

Figure 4. The effect of the crystal field on bulk states of positron orbitals within the simplified point-ionic Madelung potential. The crystal potential plays the role of the potential barrier to the positron being localized at a halide site.

Table 4. Positron annihilation lifetimes (ns) obtained for the ground state of the positron in alkali halides using the modified point-ionic and the energy band-ionic potentials.

	Point ion			Band ion			
Crystal	XO	XC	EPC	XO	XC	EPC	Experiment[a]
LiF	0.792	0.458	0.326	0.199	0.172	0.135	0.132
NaF	1.211	0.526	0.358	0.344	0.292	0.198	0.193
LiCl	1.464	1.011	0.452	0.585	0.491	0.262	0.236
NaCl	1.499	1.002	0.449	0.873	0.707	0.335	0.313

[a]Bussolati *et al* [19].

shallow crystal potential barrier of the positron.

6.2. The energy band-ionic potential model

The crystal potential is constructed by the superposition of individual ions centred at appropriate sites of the lattice. In the energy band crystal potential, each ionic site was represented by the full ionic potential on the basis of band information from the LCAO band-structure calculation [20–22]. The energy bands of alkali halides are either completely filled, or completely empty, and are separated by a large energy gap (>5 eV). Alkali halides have the ionic characteristic of the strong localization of the electron density; for example, the Na^+ ions lose their 3s electron, which is transferred to make the Cl^- ion, thereby completing the chlorine 3p shell. The 1s, 2s, and—to a large extent—also 2p levels for the Na^+ ions are so localized at the ion that for the equilibrium interatomic spacing, no

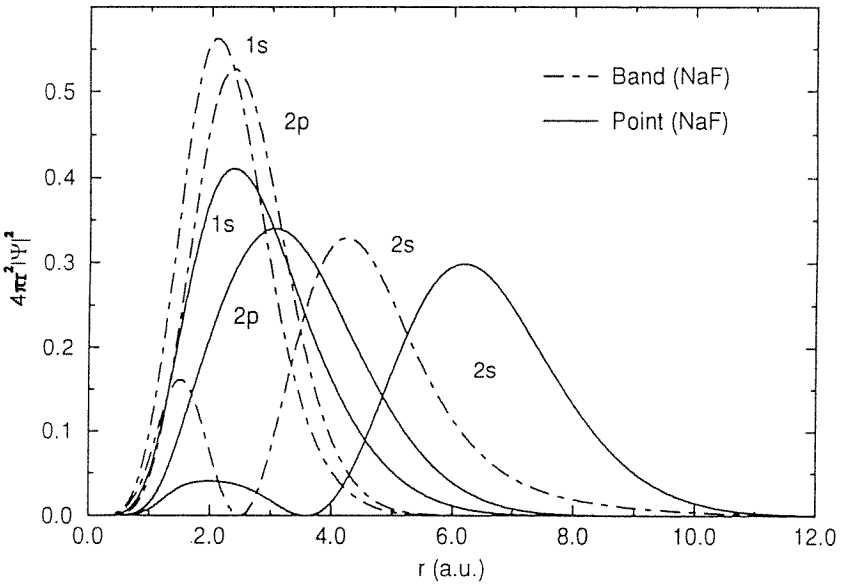

Figure 5. The model-dependent crystal effect on the bulk states of positron orbitals in the NaF crystal. The energy band crystal potential provides the potential barrier to the positron, which can be confined more tightly than in the point-ionic crystal potential case. The higher states of the positron are unphysical, due to the limitations of the single-site cluster approximation.

overlap arises, and these levels, therefore, remain atomic-like and sharp. On the other hand, there is sufficient overlap of 3s states of Na^+ ions that these build a band of levels, but this is empty. Because the Cl^- ions have large ionic radii, there is a much greater tendency for their orbitals to be overlapped. Although the more tightly bound electrons remain in sharp atomic-like states, the 3s and 3p levels of Cl^- ions are spread into relatively narrow bands. In occupied states, there is a quite small Na^+–Cl^- orbital interaction. This indicates that bands of 3s and 3p occupied levels are essentially confined wholly to the Cl^- ions. Therefore, the self-consistent density functional calculation includes 18 electrons on the halide site.

This band information has been included in the positron annihilation calculation by using the band-ionic crystal potential in the embedded-cluster method. The one-site approximation of this method facilitates this calculation just as much as it does in the modified point-ionic potential model. The positron annihilation at the anion centre, with the energy band-ionic crystal potential, is shown in table 4. On comparison with experimental results, positron lifetime calculations show a relatively good agreement for the ground state of the positron. The agreement for the calculated positron lifetimes for alkali fluorides is better than that for those for alkali chlorides. This may reflect the deeper potential well and the higher potential barrier of the crystal field to the electron and the positron, respectively, in alkali fluorides. The large discrepancy in the positron lifetimes for alkali chlorides may be attributed to the spread positron density—up to the neighbouring alkali ions—due to the shallow potential barrier of the crystal potential.

The calculations of the positron lifetimes for the ground state of the positron localized at a halide site were carried out by adding several ingredients. The XO calculations of the positron annihilation in LiF and NaF crystals using the band-ionic crystal potential predict

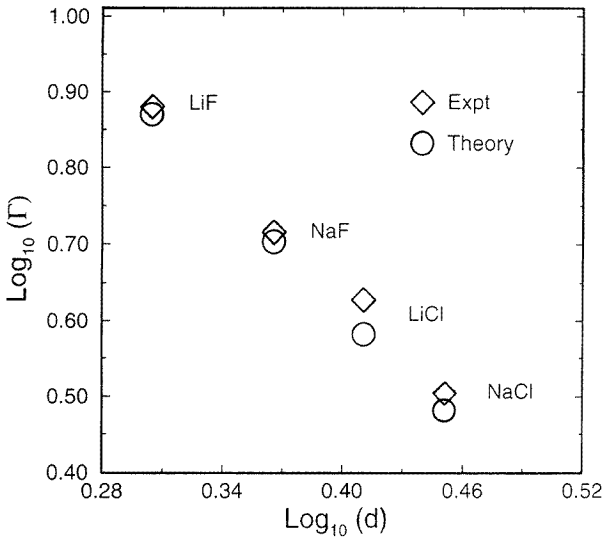

Figure 6. The power-law relation of positron annihilation rates in alkali halides; d (au) is the nearest-neighbour distance and Γ (GHz) is the annihilation rate. The experimental results from Bussolati *et al* [19] are in good agreement. The large discrepancy for LiCl is attributed to the distortion of the positron state by the neighbouring Li ion.

lifetimes that are shorter than those obtained from EPC calculations using the modified point-ionic potential. As shown in figure 5, the energy band-ionic crystal potential provides more localization of the positron density than does the point-ionic crystal potential. The ground state of the positron is strongly confined, within 5 au, which means that it is close to the adjacent ions. The higher-order positron states also show a contraction due to the strong crystal repulsion of the positron barrier. However, the states are unphysical due to the limitations of the single-site cluster approximation for the halide site. For LiCl and NaCl crystals, which have larger crystal lattice constants than LiF and NaF crystals, the details of the crystal effect are less pronounced, and the XO results are comparable with the EPC results for the modified point-ionic potential.

When the positron correlation potential in the XC calculation is taken into account in the band model, the results are only slightly changed. The inclusion of the pair correlation function in the EPC calculation also does not change the positron lifetimes much. These theoretical results agree with the experimental values well for the fully energy-minimized basis set. This implies that the strong crystal effect derived from band-structure information is the main contribution perturbing the electron and positron states. However, the effect of the positron correlation potential and the pair correlation function are not significant enough to modify the final states of both of the electrons and the positron, and thus they change the positron lifetimes only slightly.

The model dependence of the calculation of positron lifetimes is clear. The atomic calculation values obtained for the positron lifetimes—in the range 0.501–0.581 ns—become smaller on inclusion of the point-ionic crystal potential: 0.326–0.452 ns. A further reduction to values in the range 0.135–0.335 ns occurs on introducing the band-ionic crystal potential. The band potential provides an appropriate model for the 1s bound state of the positron which is well localized around the anion site. There is an interesting spectral analysis by Bertolaccini *et al* [33] of the experimental data for the annihilation rate of the shortest-lived

positron state. In their view, the crystal volume can be divided into two regions: one occupied by positive ions and the other occupied by negative ions. The density of negative ions—whose region can be accessed by the positron—is linearly dependent on the positron annihilation rate of this 1s state in highly ionic crystals. This analysis consistently agrees with the one-site approximation.

Furthermore, the positron dissociation into positronium (Ps) is not stable in the ionic crystals. The positronium formation potential ($\epsilon_{\rm Ps}$) is defined as the negative of the maximum kinetic energy of Ps atoms emitted into vacuum, and the positron affinity is the negative sum of the internal electron and positron chemical potentials [2, 34]. As a measure of the Ps dissociation, the Ps formation potential can be written in terms of the positron affinity (A_+) to the crystal:

$$\epsilon_{\rm Ps} = -A_+ - E_{\rm Ps} \tag{50}$$

where the Ps binding energy in a vacuum is $E_{\rm Ps} = -6.8$ eV. Since the positron affinity (<-7.0 eV) in the ionic crystal is strong, like in alkali metals [34], the formation potential becomes positive, which indicates the cause of the instability of the Ps. Although the Ps formation is strongly influenced by the surface state of the electron density, the strongly localized state of the electron at the surface of the ionic crystal forms a large penetration barrier against Ps escape into the vacuum.

Finally, the relationship between positron annihilation rates and crystal properties in terms of lattice constants can be addressed. As shown in figure 5, the annihilation rates (THz) for the ground state of the positron in alkali halides can be expressed using the following power laws:

$$\Gamma_{\rm theory} = 1.306 a_0^{-2.538} \tag{51}$$

$$\Gamma_{\rm exp} = 1.084 a_0^{-2.433} \tag{52}$$

where a_0 is the lattice constant. The larger the lattice constant, the less the overlap of the electron–positron densities, and thus the smaller the annihilation rates, because the positron may reside in the larger interstitial region and be longer lived.

7. Conclusions

In the pure-crystal system of alkali halides, the crystal potential has been incorporated in the Madelung ionic potentials in two ways: (1) as a modified point-ionic potential including information on the ionic radius; and (2) as a full ionic potential derived from electronic energy band-structure calculations. The density functional calculation has been performed for the anion centre in the one-site embedded scheme which includes the Hamiltonian for the infinite lattices and the Gaussian basis set at the centre. The contribution of the crystal effect competes with the positron correlation effect. The positron lifetimes are found to be sensitive to the crystal model potential used. The positron forms bound states with a substantial density in interstitial lattice positions. The positron ground state may be formed on an electron-rich anion site, and finally annihilate into two photons, in alkali halides. The results agree relatively well with experimental data, and give a power-law relationship between the annihilation lifetimes and lattice constants. The large discrepancy of positron lifetimes for the ground states in LiCl and NaCl crystals may be partially attributed to the distortion of the positron ground state caused by neighbouring alkali ions. The higher positron states are unphysical due to the limitations of the single-site cluster approximation. The inclusion of the positron interaction at alkali sites by implementing the multi-site embedded-cluster approximation is desirable.

References

[1] Kajcsos Z and Szeles C 1992 *Material Science Forum* **105–110** parts 1, 2, and 3 (Switzerland: Trans Tech)
[2] Puska M J and Nieminen R M 1994 *Rev. Mod. Phys.* **66** 841
[3] Fluss M J, Smedskjaer L C, Chason M K, Legnini D G and Siegel R W 1978 *Phys. Rev.* B **17** 3444
[4] Howell R H 1978 *Phys. Rev.* B **18** 3015
Howell R H 1981 *Phys. Rev.* B **24** 1835
[5] Simpson P J, Vos M, Mitchell I V, Wu C and Schultz P J 1991 *Phys. Rev.* B **44** 12 180
[6] Alatalo M, Nieminen R M, Puska M J, Seitsonen A P and Virkkunen R 1993 *Phys. Rev.* B **47** 6381
[7] Seitsonen A P, Virkkunen R, Puska M J and Nieminen R M 1994 *Phys. Rev.* B **49** 5253
[8] Puska M J, Sŏb M, Brauer G and Korhonen T 1994 *Phys. Rev.* B **49** 10 947
[9] Pöykkö S, Puska M J and Nieminen R M 1996 *Phys. Rev.* B **53** 3813
[10] Crawford J H Jr and Slifkin L M (ed) 1972 *Point Defects in Solids* vol I (New York: Plenum)
[11] Lauff U, Major J, Seeger A, Stoll H, Siegle A, Deckers C, Greif H, Maier K and Tongbhoyai M 1993 *Phys. Lett.* **182A** 165
[12] Schultz P J, Tandberg E, Lynn K G, Nielsen B, Jackman T E, Denhoff M W and Aers G C 1988 *Phys. Rev. Lett.* **61** 187
[13] Tandberg E, Schultz P J, Aers G C and Jackman T E 1989 *Can. J. Phys.* **67** 275
[14] Coleman P G, Chilton N B and Baker J A 1990 *J. Phys.: Condens. Matter* **2** 9355
[15] Britton D T, Willutzki D, Jackman T E and Mascher P 1992 *J. Phys.: Condens. Matter* **4** 8511
[16] Kanhere D G, Farazdel A and Smith V H Jr 1987 *Phys. Rev.* B **35** 1313
[17] Sterne P A and Kaiser J H 1991 *Phys. Rev.* B **43** 13 892
[18] Harrison J G 1986 *J. Chem. Phys.* **84** 1659
[19] Bussolati C, Dupasquier A and Zappa L 1967 *Nuovo Cimento (Ser. X)* B **52** 529
[20] Chaney R C and Lin C C 1976 *Phys. Rev.* B **13** 843
[21] Harrison J G and Lin C C 1981 *Phys. Rev.* B **23** 3894
[22] Jackson K A, Pederson M R and Harrison J G 1990 *Phys. Rev.* B **41** 12 641
[23] Ceperley D M and Alder B L 1980 *Phys. Rev. Lett.* **45** 566
[24] Perdew J P and Zunger A 1981 *Phys. Rev.* B **23** 5048
[25] Arponen J and Pajanne 1979 *Ann. Phys., NY* **121** 343
[26] Lantto L J 1987 *Phys. Rev.* B **36** 5160
[27] Boronski E and Nieminen R M 1986 *Phys. Rev.* B **34** 3820
[28] Ewald P 1921 *Ann. Phys., Lpz.* **64** 253
[29] Herman F and Skillman S 1963 *Atomic Structure Calculations* (Englewood Cliffs, NJ: Prentice-Hall)
[30] Erwin S C, Heaton R A and Lin C C 1986 *BANDAID Software Package* University of Wisconsin, Madison
[31] Ore A and Powell J L 1940 *Phys. Rev.* **75** 1696
[32] Farazdel A and Cade P E 1977 *J. Chem. Phys.* **66** 15
[33] Bertolaccini M, Bisi A, Gambarini G and Zappa L 1971 *J. Phys. C: Solid State Phys.* **4** 734
[34] Puska M J, Lanki P and Nieminen R M 1989 *J. Phys.: Condens. Matter* **1** 6081